Scar intensity statistics in the position representation

K. Damborsky and L. Kaplan
Department of Physics, Tulane University, New Orleans, Louisiana 70118, USA
(Received 17 August 2005; published 5 December 2005)

We obtain general predictions for the distribution of wave function intensities in position space on the periodic orbits of chaotic ballistic systems. The expressions depend on effective system size N, instability exponent λ of the periodic orbit, and proximity to a focal point of the orbit. Limiting expressions are obtained that include the asymptotic probability distribution of rare high-intensity events and a perturbative formula valid in the limit of weak scarring. For finite system sizes, a single scaling variable λN describes deviations from the semiclassical $N \to \infty$ limit.

DOI: 10.1103/PhysRevE.72.066204 PACS number(s): 05.45.Mt, 03.65.Sq

I. INTRODUCTION

Improving our understanding of wave function structure and transport in quantum systems with a nonintegrable classical limit, and of their relationship with the dynamics of the corresponding classical system, has been a major focus of quantum chaos research. An early and visually dramatic finding along these lines was the presence of anomalously large fluctuations in wave function intensity near the short unstable periodic orbits of the corresponding classical dynamics. In 1983, McDonald [1] observed individual wave functions (later called "scarred states") with a large excess of intensity near a particular periodic orbit, as compared with the background Gaussian random fluctuations; the completeness condition then requires other wave functions (the "antiscarred states") to have deficient intensity near the same orbit. Since that time, scars have been recognized as the one of the few visually distinctive nonrandom features of quantum chaotic wave functions, as well as possibly the leading correction to the random wave conjecture made earlier by Berry and Voros [2], which states that quantum wave function statistics should converge to the behavior of random superpositions of plane waves in the semiclassical limit of short wavelength.

The original theory of scarring was developed by Heller [3], who placed a lower bound on scar fluctuations, as measured by overlaps of wave functions with Gaussian wave packets centered on the periodic orbits. Subsequent theoretical successes included work by Bogomolny [4], who first computed an expression for scar intensity in the position representation (where scars were originally observed), and by Berry [5], who developed a parallel analysis for the Wigner functions in phase space and predicted the structure of fringe patterns decorating each orbit. In these pioneering investigations, the focus was mostly on average intensities for an energy window of nearby eigenstates, rather than on properties of individual wave functions. Later, Agam and Fishman [6] developed a semiclassical criterion for predicting scarring or antiscarring in individual wave functions. In the semiclassical limit, the phase-space region affected by the scar of any given periodic orbit tends to zero while the intensity enhancement in that region for a typical wave function remains finite; the scar effect is therefore fully consistent with the quantum ergodicity theorems of Shnirelman, Zelditch, and Colin de Verdiere [7].

Scars have been predicted and observed both experimentally and numerically in a wide variety of quantum systems with a chaotic classical limit (as well as in classical wave systems with a chaotic ray limit). Examples include applications as diverse as microwave cavities [8], hydrogen atoms in a magnetic field [9], electrons in a resonant tunneling diode with magnetic field [10], Faraday surface waves [11], vibrating soap films [12], molecular vibrations [13], and acoustic radiation [14].

In quantum or classical wave applications where dissipation effects are small enough for individual eigenstates to be resolved, it is of primary interest to study the scar effect for individual wave functions, rather than for averages over an energy or frequency window. In fact, the early empirical evidence for scarring as well as much of the empirical evidence since has been provided in the form of images of individual eigenstates. Such evidence, however, needs to be interpreted with care in light of the fact that random waves also exhibit regions of high intensity that to the eye look like scars but are in reality perfectly consistent with Gaussian random amplitude fluctuations [15]. To understand the effect of scarring on physical processes in specific systems, and even to verify the presence of this phenomenon in the first place, it is necessary to have robust quantitative predictions concerning the statistical properties of individual wave functions, which can be compared with data as well as with the Gaussian random model.

Antonsen *et al.* [16] noted that scar statistics of individual wave functions could be understood by combining known short-time dynamics associated with a given periodic orbit and random long-time recurrences whose statistical properties mirror those of random matrix theory (RMT). Similar ideas were used by Kaplan and Heller to obtain predictions for mean squared intensity on an orbit [17], and also for the full distribution of wave function intensities on or away from the orbit [18]. These predictions were obtained in a Gaussian (Husimi) phase space basis, where classical-quantum correspondence is most clearly manifest. On the other hand, wave function structure in position space is often of greater physical interest. Indeed, the original empirical evidence for scarring [1] and much subsequent numerical and experimental investigation of scarring has focused on position-space properties, in contrast with the above-mentioned theoretical work. Wave function intensities in position space are directly ac-

 ©2005 The American Physical Society

cessible, for example, in microwave cavity experiments, and in the case of a diffusive billiard, comparisons have been made with predictions based on nonlinear sigma models [19]. Such explicit comparisons between observed deviations from RMT and theoretical predictions are lacking in the ballistic case. Furthermore, a quantitative understanding of position-space wave function statistics is essential for analyzing experiments on nanostructures such as quantum dots. For example, these statistics determine the effects of electron-electron interactions on conductance peak spacings in the Coulomb blockade regime [20].

This paper is organized as follows. The inverse participation ratio, or mean squared wave function intensity, on a periodic orbit is first obtained in Sec. II, followed by an analysis of the full wave function intensity distribution in Sec. III. In both cases, accurate and robust expressions for these statistical properties are obtained that depend only on the system size, instability exponent of the periodic orbit, and proximity to a focal point. Several limiting expressions are obtained, including a result for the probability of rare high-intensity events, and a perturbative formula valid for moderate intensities when deviations from RMT are small. Finally, in Sec. IV, we compare these results with data obtained in numerical simulations, and briefly investigate the behavior of wave function statistics beyond the semiclassical regime.

II. INVERSE PARTICIPATION RATIO

We begin by considering an unstable periodic orbit of period T in d dimensions, passing through periodic point (q_0,p_0). The Van-Vleck-Gutzwiller semiclassical propagator [21] includes a contribution from this periodic orbit to the return amplitude at time $t=nT$ for position state q_0:

$$G^{\mathrm{SC}}(q_0,q_0,t)=\frac{1}{(2\pi i\hbar)^{d/2}}\left|\det\frac{\partial p(q_0,q_t)}{\partial q_t}\right|^{1/2}_{q_t=q_0} e^{in(S/\hbar-\mu\pi/2)}+\cdots. \tag{1}$$

Here S is the classical action associated with one traversal of the periodic orbit, and μ is the Maslov index, absorbing changes in the sign of the amplitude. The amplitude $|\det\partial p(q_0,q_t)/\partial q_t|^{1/2}_{q_t=q_0}$, where p is the initial momentum needed to travel from fixed q_0 to q_t in time t, is evaluated for the return trajectory $q_t=q_0$, and is the square root of the corresponding classical focusing factor. Of course, q_0, p, and q_t are all d-component vectors in the general case. Omitted terms in Eq. (1) are associated with other classical paths of length t beginning and ending at the same point q_0; as we will see below the periodic path dominates the statistics of individual wave functions when the instability exponent of this periodic path is small. For sufficiently short times t or sufficiently small $\hbar$, $G^{\mathrm{SC}}(q_0,q_0,t)$ is a good approximation to the true quantum return amplitude $G(q_0,q_0,t)$.

For simplicity of presentation, and for easy comparison with numerical results in Sec. IV, we now restrict ourselves to the case of discrete-time maps, which are commonly used as models for more general chaotic dynamical systems [22]. One-dimensional maps may be obtained by stroboscopically viewing a one-dimensional system with time-dependent Hamiltonian (such as the kicked rotator or standard map [23]), or alternatively by taking a Poincaré surface of section for a two-dimensional time-independent Hamiltonian (such as a hard-wall billiard or smooth two-dimensional potential). For a one-dimensional map on a compact phase space of area 1, the quantum vector space is spanned by a finite basis of $N=1/2\pi\hbar$ independent position states $|q_i\rangle$. Conventionally, we adopt a wave function normalization where the average of the discrete wave function intensities is set to unity: $\Sigma_{i=0}^{N-1}|\Psi(q_i)|^2=N$, and the propagator $G(q_t,q,t)$ becomes a unitary N by N matrix. With this normalization,

$$G^{\mathrm{SC}}_{\mathrm{map}}(q_0,q_0,t)=\begin{cases}\dfrac{1}{(iN)^{1/2}}\left|\dfrac{\partial p(q_0,q_t)}{\partial q_t}\right|^{1/2}_{q_t=q_0} e^{in(S/\hbar-\mu\pi/2)}+\cdots & n>0\\ 1 & n=0\end{cases}, \tag{2}$$

where $n=t/T$ is an integer. Furthermore, for a $d=1$ map, or equivalently for a $d=2$ continuous-time dynamics, the monodromy matrix of the unstable periodic orbit is simply a 2 by 2 matrix, and may be written as

$$\begin{pmatrix}\partial q_t(q,p)/\partial q & \partial q_t(q,p)/\partial p\\ \partial p_t(q,p)/\partial q & \partial p_t(q,p)/\partial p\end{pmatrix}=\begin{pmatrix}a & b\\ c & d\end{pmatrix}\begin{pmatrix}e^{n\lambda} & 0\\ 0 & e^{-n\lambda}\end{pmatrix}\times\begin{pmatrix}d & -b\\ -c & a\end{pmatrix}, \tag{3}$$

where all partial derivatives are evaluated at the periodic point $(q,p)=(q_0,p_0)$, area preservation implies $ad-bc=1$, and $\lambda>0$ is the dimensionless positive instability exponent for one iteration of the periodic orbit. Then the inverse of the focusing factor in Eq. (2) becomes

$$(|\partial p(q_0,q_t)/\partial q_t|_{q_t=q_0})^{-1}=|\partial q_t(q_0,p)/\partial p|_{q_t=q_0}=2|ab\sinh(\lambda t/T)|. \tag{4}$$

We are interested in the effect of the unstable periodic orbit on individual wave function behavior at or near q_0, and specifically on the wave function intensities $|\Psi(q_0)|^2$. A general discussion of the intensity distribution $\mathcal{P}(|\Psi(q_0)|^2)$ is deferred until Sec. III; here we focus first on the mean squared intensity, also known as the inverse participation ratio (IPR),

$$\mathcal{I}(q_0)=\overline{|\Psi(q_0)|^4}, \tag{5}$$

where the average $\bar{\cdots}$ is performed over eigenstates of the system, and the mean intensity $\overline{|\Psi(q_0)|^2}$ is normalized to unity as above. For a general Hamiltonian system, the average must be restricted to a classically narrow energy window; in the case of a discrete-time map, however, we are free to average over all values of the (periodic) quasienergy. $\mathcal{I}(q_0)$ is the inverse fraction of wave functions in the energy window that have significant intensity at q_0; its possible values range from 1 in the case of complete ergodicity (where every wave function has equal intensity at q_0) to N in the

case of complete localization (where the wave functions are delta functions in position space).

As has previously been discussed [24], for a nondegenerate system the IPR is proportional to the long-time return probability for initial state $|q_0\rangle$, which for the chaotic case is in turn proportional to a sum of return probabilities due to the periodic orbit,

$$\mathcal{I}(q_0) = \mathcal{N}\int_{-\infty}^{\infty} dt |G_{\rm map}(q_0,q_0,t)|^2 \approx F\frac{\sum_{n=-\infty}^{\infty} |G^{\rm p.o.}_{\rm map}(q_0,q_0,nT)|^2}{|G^{\rm p.o.}_{\rm map}(q_0,q_0,0)|^2}. \tag{6}$$

Here $G^{\rm p.o.}_{\rm map}$ is the contribution to the propagator from a single dominant periodic orbit, as given in Eq. (1), and $\mathcal{N}$ is a normalization constant. The multiplicative factor F encodes information about all recurrences not included in $G^{\rm p.o.}_{\rm map}$; semiclassically these recurrences are associated with closed classical trajectories other than the original periodic orbit. Treating these other contributions as random and uncorrelated, which is physically justifiable for chaotic dynamics at long times, leads to the random wave result $F=3$ (for real wave functions, in the presence of time reversal symmetry) or $F=2$ (for complex wave functions, in the absence of time reversal symmetry).

Combining the results of Eqs. (2), (4), and (6), we obtain the prediction

$$\mathcal{I}_{\rm pred}(q_0) = F\left[1 + \sum_{n\neq 0} \frac{1}{2N|ab\sinh(\lambda n)|}\right] = F\left[1 + \frac{1}{N|ab|}\sum_{n=1}^{\infty}\frac{1}{\sinh(\lambda n)}\right]. \tag{7}$$

For instability exponent $\lambda \gg 1$, only one iteration of the orbit contributes, and we obtain $\mathcal{I}_{\rm pred}(q_0)=F[1+(2/N|ab|)e^{-\lambda}]$, converging eventually to the random wave result $\mathcal{I}_{\rm RMT}(q_0)=F$. In the more interesting limit $\lambda \ll 1$, we obtain

$$\sum_{n=1}^{\infty}\frac{1}{\sinh(\lambda n)} \approx \sum_{n=1}^{M}\frac{1}{\lambda n} + \int_M^{\infty}\frac{dn}{\sinh(\lambda n)} \approx \frac{1}{\lambda}\left(\ln\frac{1}{\lambda} + \gamma + \ln 2\right), \tag{8}$$

where $1 \ll M \ll \lambda^{-1}$ and $\gamma \approx 0.577$ is Euler's constant. Then we find

$$\mathcal{I}_{\rm pred}(q_0) = F\left[1 + \frac{1}{\lambda|ab|N}\left(\ln\frac{2}{\lambda} + \gamma\right)\right] \tag{9}$$

in the weakly unstable regime $\lambda \ll 1$.

From Eq. (7) or Eq. (9), we see that scar strength, as measured by the inverse participation ratio, depends on three parameters only: the semiclassical parameter N (or ratio of system size to wavelength), the instability exponent λ of the periodic orbit, and the phase space orientation parameter $|ab|$, which is directly related to the angle between the p axis and the unstable manifold of the orbit at the point (q_0,p_0). In a two-dimensional Hamiltonian system, such as a billiard or smooth potential, the stable manifold rotates and the $|ab|$ parameter changes as one moves along the orbit, approaching zero at the focal points. Thus all possible values of $|ab|$ are relevant for describing the wave function behavior near a generic orbit, while λ is a constant parameter for a fixed orbit. For small values of $|ab|$, which correspond to the strongest scarring, $|ab|$ is directly proportional to the distance from the nearest focal point on the orbit. In a specific discrete-time map, $|ab|$ has a single value for each orbit of period 1, since each such orbit has only one periodic point. However, the same correspondence between the $|ab|$ parameter and distance to a focal point applies also in the case of maps, if we consider a *family* of maps arising from Poincaré sections intersecting a given orbit at various distances from a focal point.

We need to understand the range of validity for Eq. (7) or Eq. (9). Classical-quantum correspondence $G(q_0,q_0,t) \approx G^{\rm SC}(q_0,q_0,t)$ fails when q_0 is within a wavelength of a focal point, as the classically singular probability density is smoothed out by the uncertainty principle. Thus our semiclassical derivation fails for $|ab|<N^{-1}$, and the correct scaling behavior for this regime must be obtained by replacing $|ab|N$ with a number of order unity. Thus the inverse participation ratio $\mathcal{I}(q_0)$ remains finite at $O(\lambda^{-1})$ for $\lambda \ll 1$ as $|ab|N \to 0$. We note that the IPR scales as λ^{-1} in the basis of phase-space Gaussians optimally oriented with respect to the stable and unstable manifolds of the periodic orbit [17]; it is not surprising to obtain the same scaling behavior in position space near the focal points of the orbit, since a position state in this case may be thought of simply as a limiting case of a family of optimal Gaussians.

A second limitation on the validity of Eq. (7) or Eq. (9) is that the Lyapunov time T/λ needed to escape from the vicinity of the orbit must be much shorter than the Heisenberg time N, at which quantum mechanical exploration ceases and the quantum dynamics becomes quasiperiodic. For $\lambda N < T$, the infinite sum in Eq. (7) must be cut off at $n \sim N/T$ to avoid counting classical recurrences that occur after the Heisenberg time and have no quantum analog. This has the effect of replacing λN in Eq. (9) with a constant of order T when $\lambda N < T$, so that the inverse participation ratio again remains finite: $\mathcal{I}(q_0) \sim |ab|^{-1}T^{-1}$ as $\lambda \to 0$. The behavior of the IPR for $\lambda N < T$ will be discussed further in Sec. IV. For $\lambda \to 0$ and $|ab| \to 0$ simultaneously, the IPR must obey an upper bound $\mathcal{I}(q_0) \leq N$, which is saturated only if the position state $|q_0\rangle$ is itself an eigenstate of the dynamics.

In conclusion, for a given semiclassical parameter N, we require $|ab| > N^{-1}$ and $\lambda > TN^{-1}$ for our semiclassical expressions to be valid; smaller values of λ or $|ab|$ do not lead to parametrically stronger scarring. At the same time, as seen from Eq. (9), we need simultaneously $\lambda \ll 1$ and $|ab| \ll 1$ to obtain a large enhancement of the IPR above the RMT prediction. We also note that in any specific dynamical system, multiple trajectories (periodic or closed) contribute to $\mathcal{I}(q_0)$ at order N^{-1}, and a single orbit can only be expected to dominate the wave function statistics at q_0 when $|ab| \ll 1$ and $\lambda \ll 1$, i.e., when q_0 is close to a focal point of a weakly unstable periodic orbit.

III. SCAR INTENSITY DISTRIBUTION

Although the IPR provides a useful one-number measure of the degree of wave function localization at q_0, it is only

the lowest nontrivial moment of the intensity distribution, and as such provides limited information about the full distribution. In particular, $\mathcal{I}(q_0) > \mathcal{I}_{\mathrm{RMT}} = F$ implies an increased intensity variance and clearly suggests longer tails of the intensity distribution, i.e., an enhanced probability of finding wave functions with intensity $I = |\Psi(q_0)|^2$ much larger or much smaller than the average intensity. However, to obtain quantitative predictions about the probability of such rare events, we must go beyond the IPR to examine the full intensity distribution $\mathcal{P}(I)$.

As in Sec. II, we assume a clear separation of scales exists between known short-time recurrences associated with a particular short periodic orbit and new long-time nonlinear recurrences which semiclassically may be associated with an exponentially large number of homoclinic paths starting and ending near q_0. The statistical properties of these new recurrences at long times may be assumed to be consistent with RMT, i.e., independent of the fact that q_0 happens to lie on a short periodic orbit [17]. The full return amplitude at long times then becomes a convolution of the known short-time dynamics and the RMT-like random long-time recurrences [17]:

$$G_{\mathrm{map}}(q_0, q_0, t) \approx \sum_{\tau} G^{\mathrm{p.o.}}_{\mathrm{map}}(q_0, q_0, \tau) G^{\mathrm{rnd}}(q_0, q_0, t - \tau). \tag{10}$$

Fourier transforming, we find that the local density of states at q_0 is given by the product of a smooth envelope associated with the periodic orbit and a random fluctuating part:

$$\sum_{\alpha} |\Psi_\alpha(q)|^2 \delta(E - E_\alpha) = \widetilde{G}_{\mathrm{map}}(q_0, q_0, E) = \widetilde{G}^{\mathrm{p.o.}}_{\mathrm{map}}(q_0, q_0, E) \sum_{\alpha} |r_\alpha|^2 \delta(E - E_\alpha), \tag{11}$$

where the r_α are distributed as (real or complex) independent Gaussian random variables with mean 0 and variance 1, and $G^{\mathrm{p.o.}}_{\mathrm{map}}(q_0, q_0, E)$ is the Fourier transform of Eq. (2). The individual wave function intensities are given by

$$I_\alpha = |\Psi_\alpha(q_0)|^2 = \widetilde{G}^{\mathrm{p.o.}}_{\mathrm{map}}(q_0, q_0, E_\alpha) |r_\alpha|^2 = S(E_\alpha) |r_\alpha|^2, \tag{12}$$

where we have given the name $S(E)$ to the smooth part of the local density of states at q_0. Explicitly, this smooth envelope coming from the short periodic orbit takes the form

$$S(E) = 1 + 2 \frac{1}{\sqrt{2N|ab|}} \sum_{n=1}^{\infty} \frac{1}{\sqrt{\sinh(\lambda n)}} \times \cos\left(\frac{n(ET + S)}{\hbar} - \frac{n\mu\pi}{2} - \frac{\pi}{4} \right). \tag{13}$$

The full intensity distribution at q_0 is given by an energy average. Since the level density is constant for a map (and constant within the energy window of interest for a continuous-time Hamiltonian system), and the random factors $|r_\alpha|^2$ are uncorrelated with the smooth envelope $S(E)$, each moment of the intensity distribution may be obtained as a product of a factor depending on properties of the orbit and a universal factor associated with Gaussian random fluctuations:

$$\overline{I^s} = \left(\frac{1}{2\pi\hbar/T} \int_{E_1}^{E_1 + 2\pi\hbar/T} dE (S(E))^s \right) \cdot (\overline{|r_\alpha|^{2s}}). \tag{14}$$

Note that the smooth envelope is periodic in T, so we need only to average over the energy interval $E_1 \leqslant E \leqslant E_1 + 2\pi\hbar/T$. In particular, using $\overline{I^2} = \mathcal{I}(q_0)$, $\overline{|r_\alpha|^4} = F$, and Eq. (13), we recover the result of Eq. (7) for the inverse participation ratio.

In the absence of time-reversal symmetry, r_α is a complex Gaussian and the random factor in Eq. (12) is exponentially distributed,

$$\mathcal{P}(|r_\alpha|^2) = e^{-|r_\alpha|^2}, \tag{15}$$

while in the presence of time-reversal symmetry r_α is real and its square follows a Porter-Thomas distribution,

$$\mathcal{P}_{\mathrm{TRS}}(|r_\alpha|^2) = \frac{1}{\sqrt{2\pi|r_\alpha|^2}} e^{-|r_\alpha|^2/2}. \tag{16}$$

For definiteness, we focus on the generic situation of no time-reversal symmetry. At a fixed energy E, the distribution of $I = S(E)|r_\alpha|^2$ is $\mathcal{P}(I) = [1/S(E)] e^{-I/S(E)}$, and the combined intensity distribution over all energies is

$$\mathcal{P}(I) = \frac{1}{2\pi\hbar/T} \int_{E_1}^{E_1 + 2\pi\hbar/T} \frac{dE}{S(E)} e^{-I/S(E)}. \tag{17}$$

Several limits are of particular interest. If the scarring is relatively weak, i.e., $S(E) - 1 \ll 1$ in Eq. (13), we may expand Eq. (17) to second order in $S(E) - 1$ to obtain

$$\mathcal{P}(I) = \left(1 + \epsilon - 2\epsilon I + \frac{\epsilon}{2} I^2 + O(\epsilon^2) \right) e^{-I}, \tag{18}$$

in complete analogy with perturbative results for disordered systems, in the limit of weak disorder [25]. Here

$$\epsilon = \frac{1}{2\pi\hbar/T} \int_{E_1}^{E_1 + 2\pi\hbar/T} dE (S(E))^2 = \frac{\mathcal{I}(q_0)}{F} - 1 = \frac{\mathcal{I}(q_0) - 2}{2}, \tag{19}$$

and for $\epsilon \to 0$ we recover the Porter-Thomas distribution predicted by random matrix theory: $\mathcal{P}_{\mathrm{RMT}}(I) = e^{-I}$. In the perturbative regime, deviations of the intensity distribution from the RMT prediction are proportional to the deviation of the IPR from its RMT value of 2. We note that the validity of Eq. (18) requires $I \ll 1$ in addition to $I\epsilon \ll 1$, so perturbation theory does not apply in the tail of the intensity distribution.

To obtain a simple expression for the probability of rare events, i.e., intensities much higher than the average intensity $\overline{I} = 1$, we need to follow a different approach. For large I, the integral in Eq. (17) may be evaluated using the saddle point (stationary phase) method, with the dominant contribution coming from the energy at which the smooth envelope $S(E)$ is peaked. Physically, this means that very large wave function intensities will almost always be at the "scar ener-

gies" E_0 where interference from successive iterations of the orbit add fully constructively, and never at the "antiscar energies" where this interference is destructive. We then obtain

$$\mathcal{P}(I) = \frac{1}{2\pi\hbar/T}\sqrt{\frac{2\pi}{|S''(E_0)|I}}e^{-I/S(E_0)}, \tag{20}$$

where E_0 is the energy at which the smooth envelope $S(E)$ of Eq. (13) is peaked, and $S(E_0)$ and $S''(E_0)$ are the value and the second derivative of $S(E)$ at the peak.

For small λ, we may rewrite the sum in Eq. (13) as an integral, which may be evaluated in terms of hypergeometric functions. We then find that the smooth local density of states is peaked at

$$E_0 \approx \frac{-S + \mu\pi\hbar/2 + \beta\lambda\hbar}{T}, \tag{21}$$

where the dimensionless constant $\beta \approx 0.2133$ is the solution of $\int_0^\infty dx\, x \sin(\beta x - \pi/4)/\sqrt{\sinh x} = 0$. The height of the peak is given in this limit by

$$S(E_0) \approx \sqrt{\frac{2}{N|ab|}}\frac{\gamma}{\lambda}, \tag{22}$$

while the second derivative is

$$S''(E_0) \approx -\sqrt{\frac{2}{N|ab|}}\frac{T^2}{\hbar^2}\frac{\delta}{\lambda^3}, \tag{23}$$

where $\gamma = \int_0^\infty dx \cos(\beta x - \pi/4)/\sqrt{\sinh x} \approx 3.059$ and $\delta = \int_0^\infty dx x^2 \cos(\beta x - \pi/4)/\sqrt{\sinh x} \approx 16.14$ are dimensionless constants. Combining these results, the tail of the intensity distribution for small λ finally takes the form

$$\mathcal{P}(I) \approx \sqrt{\frac{\lambda^3}{2\pi\delta A I}}e^{-\lambda I/\gamma A}, \tag{24}$$

where $A = \sqrt{2/N|ab|}$ is a geometrical factor that becomes O(1) near a focal point of the periodic orbit. Comparing with $\mathcal{P}_{\mathrm{RMT}}(I) = e^{-I}$, we note that the tail of the intensity distribution remains exponential in the presence of scarring, but the exponent now depends on the instability exponent λ, leading to a greatly enhanced probability of finding very high wave function intensities on weakly unstable orbits. The exponentially small probability of rare events in *ballistic* chaotic systems, as given by Eq. (24), contrasts with the log-normal tail predicted and observed for *diffusive* two-dimensional systems in the metallic regime [25].

In the opposite limit $I \to 0$, Eq. (17) implies $\mathcal{P}(I) \to \overline{S^{-1}} > 1/\bar{S} = 1 = \mathcal{P}_{\mathrm{RMT}}(I)$; this enhanced probability of very small intensities is known as the antiscar effect.

IV. NUMERICAL MODEL AND RESULTS

For the purpose of testing the general results obtained in Sec. II and III, we consider a specific family of discrete-time kicked maps defined classically on a toroidal phase space $(q,p) \in [0,1) \times [0,1)$. The time evolution for one step $(q_n, p_n) \to (q_{n+1}, p_{n+1})$ is given by

$$\begin{aligned} q_{n+1/2} &= q_n + T_1'(p_n) \bmod 1, \\ p_{n+1} &= p_n - V'(q_{n+1/2}) \bmod 1, \\ q_{n+1} &= q_{n+1/2} + T_2'(p_{n+1}) \bmod 1 \end{aligned} \tag{25}$$

with

$$\begin{aligned} T_1(p) &= \frac{1}{2}(p-p_0)^2 + D_1[2\sin 2\pi(p-p_0) \\ &\quad - \sin 4\pi(p-p_0)], \\ V(q) &= -\frac{1}{2}K_q(q-q_0)^2 + D_2K_q[2\sin 2\pi(q-q_0) \\ &\quad - \sin 4\pi(q-q_0)], \\ T_2(p) &= \frac{1}{2}K_p(p-p_0)^2 + D_3K_p[2\sin 2\pi(p-p_0) \\ &\quad - \sin 4\pi(p-p_0)]. \end{aligned} \tag{26}$$

Physically, such a map may be thought of arising from a time-periodic Hamiltonian where a particle experiences free evolution under the influence of kinetic term $T_1(p)$ for the first half of a period, followed by a sudden kick of strength $V(q)$ and then by additional free evolution with kinetic term $T_2(p)$ for the second half of the period. The corresponding quantum evolution for one step is given by

$$\hat{U} = e^{-iT_2(\hat{p})/\hbar}e^{-iV(\hat{q})/\hbar}e^{-iT_1(\hat{p})/\hbar}, \tag{27}$$

where $\hbar = 1/2\pi N$, and N is the dimension of the Hilbert space. If we were interested in the spectral behavior only, we could of course view the same dynamics stroboscopically right before or right after each kick, effectively combining the two free evolution substeps into one governed by kinetic term $T_1 + T_2$. In that case, choosing $q_0 = p_0 = 0$ and integer values for K_q and K_p [so that both $V'(q)$ and $T_2'(p)$ are continuous functions on the torus] would correspond to a perturbed cat map, a system well studied in the literature [26].

In our case, we choose noninteger values of K_q and K_p, as well as generic values for q_0 and p_0, resulting in diffraction at $q = 0$ and $p = 0$. Nonzero q_0 and p_0 also cause a breaking of time-reversal symmetry. By construction, the above map is fully chaotic, for positive K_q and $K_p + 1$, and has a periodic orbit of period $T = 1$ at $(q,p) = (q_0, p_0)$. The instability exponent λ and unstable manifold orientation parameter $|ab|$ of this orbit are implicitly determined by the parameters K_q and K_p via the relations

$$\begin{aligned} 2\cosh\lambda &= 2 + K_q(1+K_p), \\ 2|ab|\sinh\lambda &= 1 + K_p(1+K_q). \end{aligned} \tag{28}$$

Any desirable values of λ and $|ab|$ may be obtained by selecting appropriate K_q and K_p in accordance with Eq. (28). The parameters D_1, D_2, and D_3 have no effect on the unstable orbit at (q_0, p_0) or on its monodromy matrix [Eq. (3)], and within certain bounds these additional parameters do not

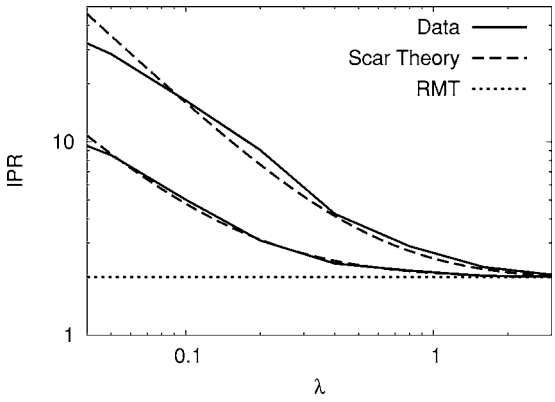

FIG. 1. The average inverse participation ratio $\mathcal{I}(q_0)$ on a periodic orbit is shown as a function of instability exponent λ of the periodic orbit, for the system defined by Eqs. (25) and (26) with system size $N=1024$. The upper and lower curves correspond to $|ab|=0.005$, 0.025, respectively. The scar theory prediction of Eq. (9) with $F=2$ is indicated by dashed lines. All quantities shown in this and subsequent figures are dimensionless.

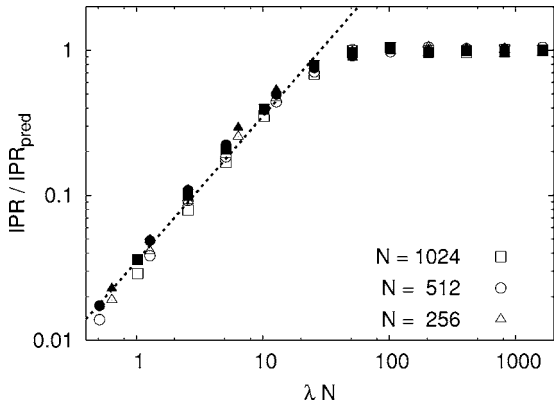

FIG. 2. $f(\lambda N)$ [Eq. (29)], the ratio of the observed inverse participation ratio to the asymptotic prediction of Eq. (9), is shown as a function of scaling parameter λN, for three different system sizes. Open and filled symbols represent $|ab|=0.025$ and 0.05, respectively. The dotted line indicates the asymptotic behavior $f(\lambda N) \approx 0.035\,\lambda N$, for $\lambda N \ll 1$.

affect the fully chaotic nature of the dynamics [26]. Such additional parameters may be used to construct a large ensemble of distinct classical systems with identical linearized behavior near the dominant periodic orbit. In our numerical investigations, however, we did not see significant effects in wave function statistics due to variation of D_1, D_2, and D_3, and for simplicity the data shown below was collected using $D_1=D_2=D_3=0$. For a given pair of parameters K_q, K_p (equivalently, $\lambda, |ab|$), we do generate an ensemble of similar systems by varying q_0 and p_0, as well as varying boundary conditions in both the q and p directions. Specifically, the boundary condition variation is accomplished by taking parameters ϵ_1 and ϵ_2 uniformly distributed between 0 and 1, and requiring $\Psi(q+1)=\Psi(q)e^{-i2\pi\epsilon_1}$ and $\tilde{\Psi}(p+1)=\tilde{\Psi}(p)e^{i2\pi\epsilon_2}$; this is equivalent to the choice $q_j=(j+\epsilon_2)/N$, $0\leqslant j\leqslant N-1$ for the position-space basis and $p_\ell=(\ell+\epsilon_1)/N$, $0\leqslant \ell\leqslant N-1$ for the momentum-space basis.

In Fig. 1, we examine the IPR as a function of the instability exponent λ of the periodic orbit, for two values of $|ab|$. Good agreement is observed with the simple asymptotic expression given by Eq. (9) for a wide range of parameters, as the size of the observed and predicted fluctuations varies by an order of magnitude. We recall that the validity of Eq. (9) requires $N^{-1}\ll\lambda\ll 1$, since the orbit period $T=1$ in the present case. Figure 2 shows what happens to the IPR as we leave the semiclassical limit $N^{-1}\ll\lambda$. We observe that to a very good approximation, deviations from the semiclassical prediction are well described by a simple scaling variable λN:

$$\mathcal{I}(q_0) = f(\lambda N)\mathcal{I}_{\text{pred}}(q_0), \tag{29}$$

where $\mathcal{I}_{\text{pred}}(q_0)$ is the asymptotic prediction of Eq. (9), $f(x)\to 1$ for $x\gg 1$, and $f(x)\sim x$ for $x\ll 1$ (as indicated by the dotted line in Fig. 2). The dimensionless parameter λN may equivalently be expressed as the ratio T_H/T_λ, where T_H is the Heisenberg time at which individual eigenstates are resolved and $T_\lambda=1/\lambda$ is a Lyapunov time associated with classical decay away from the periodic orbit. It is noteworthy that the crossover between the semiclassical behavior at large λN and the saturated behavior at small λN occurs around $\lambda N\approx 40$ for all parameter values considered. This implies, for example, that in applications to quantum dots in the Coulomb blockade regime, where $30\leqslant N\leqslant 70$ in some typical experiments [27], asymptotic $N\to\infty$ expressions are inadequate for describing wave function intensity statistics in "generic" chaotic mean-field potentials ($\lambda\sim 1$), and finite-$\hbar$ expressions must be used instead. Accurate modeling of wave function statistical properties in such systems is necessary for proper understanding and interpretation of conductance peak spacing experiments [20].

We now turn to the full distribution of wave function intensities. A typical probability distribution is shown in Fig. 3, and the scar theory prediction of Eq. (17) clearly describes the data much better than does the random matrix theory result. We note that the distribution of rare high-intensity

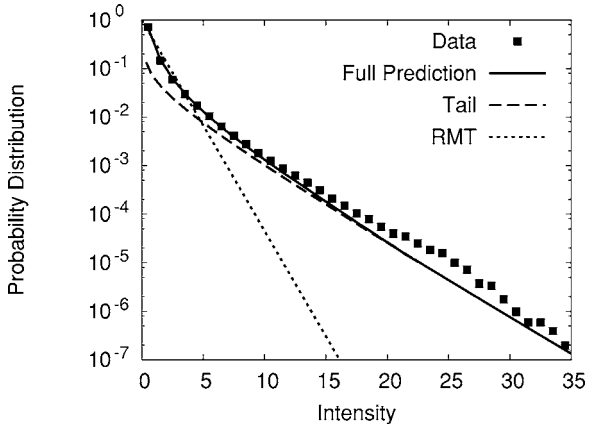

FIG. 3. The wave function intensity distribution for $N=512$, $\lambda=0.9$, and $|ab|=0.005$ is compared with the scar theory prediction of Eq. (17) (solid line) and with the simpler expression of Eq. (24) (dashed line), which is valid for large intensities. The random matrix result $\mathcal{P}_{\text{RMT}}(I)=e^{-I}$ is shown by a dotted line for comparison.

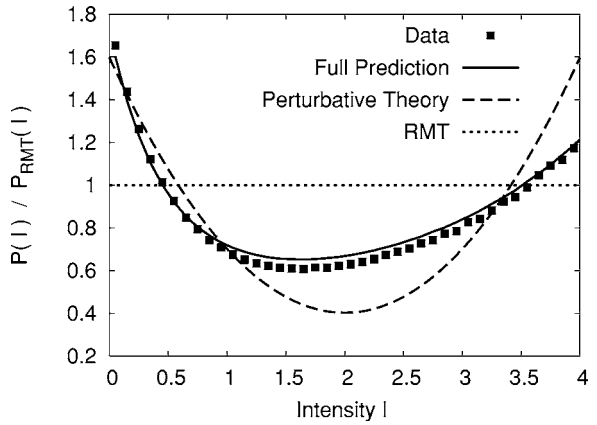

FIG. 4. The wave function intensity distribution $\mathcal{P}(I)$ is scaled by the random matrix theory prediction $\mathcal{P}_{\mathrm{RMT}}(I)$, and the result is compared with the full prediction of Eq. (17) and the perturbative limit of Eq. (18). All parameters are the same as in the previous figure.

events is in adequate quantitative agreement with the simple "tail" formula of Eq. (24), although the latter result is strictly valid only in the $\lambda \to 0$ limit. In Fig. 4, we see that the scar theory prediction also works well in the region of small to moderate intensities; in particular it correctly predicts the antiscar enhancement for $I \ll 1$. The parameters used here are evidently outside the range of validity of the perturbative expression [Eq. (18)]. For the values of N and $|ab|$ considered in Fig. 4, the perturbative result becomes applicable in the main body of the distribution for $\lambda \geqslant 1.5$ (not shown), where the system is sufficiently unstable that deviations from RMT fall below the 20% level.

V. SUMMARY

We have studied the distribution of position-space wave function intensities on an unstable periodic orbit in a ballistic chaotic system. In the two-dimensional case (equivalently, in a one-dimensional discrete-time map), the full distribution of intensities is given by three parameters: (i) the system size in wavelength units, or alternatively the dimensionless conductance, inverse effective $\hbar$, or Heisenberg time in units of a one-bounce time; (ii) the instability exponent of the periodic orbit; and (iii) orientation of the unstable manifold or alternatively the proximity to a focal point. Generalization to higher dimensions is straightforward.

The tail of the probability distribution is exponential, with exponent proportional to a simple function of the above three parameters. This contrasts with the log-normal distribution of rare events in disordered two-dimensional systems. When the scar effect is weak, the behavior for moderate intensities is given by a perturbative expression in complete analogy with the disordered case.

Simple semiclassical expressions begin to break down when the classical Lyapunov time associated with decay away from the periodic orbit reaches 2.5–3 % of the Heisenberg time. A better quantitative understanding of these saturation effects is needed for reliable predictions of wave function statistics in finite-size ballistic systems.

ACKNOWLEDGMENT

This work was supported in part by Louisiana Board of Regents Support Fund Contract No. LEQSF(2004-07)-RD-A-29.

[1] S. W. McDonald, Lawrence Berkeley Laboratory Report No. LBL-14837, 1983 (unpublished).
[2] M. V. Berry, J. Phys. A **10**, 2083 (1977); A. Voros, in *Stochastic Behavior in Classical and Quantum Hamiltonian Systems*, edited by G. Casati and J. Ford, Lecture Notes in Physics Vol. 93 (Springer, Berlin, 1979), p. 326.
[3] E. J. Heller, Phys. Rev. Lett. **53**, 1515 (1984).
[4] E. B. Bogomolny, Physica D **31**, 169 (1988).
[5] M. V. Berry, Proc. R. Soc. London, Ser. A **423**, 219 (1989).
[6] O. Agam and S. Fishman, Phys. Rev. Lett. **73**, 806 (1994).
[7] A. I. Shnirelman, Usp. Mat. Nauk **29**, 181 (1974); Y. Colin de Verdiére, Commun. Math. Phys. **102**, 497 (1985); S. Zelditch, Duke Math. J. **55**, 919 (1987); S. Zelditch and M. Zworski, Commun. Math. Phys. **175**, 673 (1996).
[8] S. Sridhar, Phys. Rev. Lett. **67**, 785 (1991).
[9] D. Wintgen and A. Hönig, Phys. Rev. Lett. **63**, 1467 (1989); K. Müller and D. Wintgen, J. Phys. B **27**, 2693 (1994).
[10] P. B. Wilkinson, T. M. Fromhold, L. Eaves, F. W. Sheard, N. Miura, and T. Takamasu, Nature (London) **380**, 608 (1996).
[11] O. Agam and B. L. Altshuler, Physica A **302**, 310 (2001); A. Kudrolli, M. C. Abraham, and J. P. Gollub, Phys. Rev. E **63**, 026208 (2001).
[12] E. Arcos, G. Baez, P. A. Cuatlayol, M. L. H. Prian, R. A. Mendez-Sanchez, and H. Hernandez-Saldana, Am. J. Phys. **66**, 601 (1998).
[13] F. J. Arranz, F. Borondo, and R. M. Benito, Phys. Rev. Lett. **80**, 944 (1998).
[14] D. Delande and D. Sornette, J. Acoust. Soc. Am. **101**, 1793 (1997).
[15] P. O'Connor, J. Gehlen, and E. J. Heller, Phys. Rev. Lett. **58**, 1296 (1987).
[16] T. M. Antonsen, Jr., E. Ott, Q. Chen, and R. N. Oerter, Phys. Rev. E **51**, 111 (1995).
[17] L. Kaplan and E. J. Heller, Ann. Phys. (N.Y.) **264**, 171 (1998); Phys. Rev. E **59**, 6609 (1999).
[18] L. Kaplan, Phys. Rev. Lett. **80**, 2582 (1998).
[19] A. Kudrolli, V. Kidambi, and S. Sridhar, Phys. Rev. Lett. **75**, 822 (1995).
[20] D. Ullmo and H. U. Baranger, Phys. Rev. B **64**, 245324 (2001); Y. Alhassid and S. Malhotra, *ibid.* **66**, 245313 (2002).
[21] M. C. Gutzwiller, J. Math. Phys. **12**, 343 (1971).
[22] S. Fishman, D. R. Grempel, and R. E. Prange, Phys. Rev. Lett. **49**, 509 (1984); A. Altland and M. R. Zirnbauer, *ibid.* **77**, 4536 (1996).
[23] B. V. Chirikov, Phys. Rep. **52**, 264 (1979).

[24] L. Kaplan and E. J. Heller, Phys. Rev. E **62**, 409 (2000).
[25] A. Mirlin, Phys. Rep. **326**, 259 (2000).
[26] P. A. Boasman and J. P. Keating, Proc. R. Soc. London, Ser. A **449**, 629 (1995).
[27] U. Sivan, R. Berkovits, Y. Aloni, O. Prus, A. Auerbach, and G. Ben-Yoseph, Phys. Rev. Lett. **77**, 1123 (1996); S. R. Patel, S. M. Cronenwett, D. R. Stewart, A. G. Huibers, C. M. Marcus, C. I. Duruöz, J. S. Harris, Jr., K. Campman, and A. C. Gossard, *ibid.* **80**, 4522 (1998);S. Lüscher, T. Heinzel, K. Ensslin, W. Wegscheider, and M. Bichler, *ibid.* **86**, 2118 (2001); F. Simmel, T. Heinzel, and D. A. Wharam, Europhys. Lett. **38**, 123 (1997).